

Article

Cation Dependence of Crystal Structure and Band Parameters in a Series of Molecular Conductors, β' -(Cation)[Pd(dmit)₂]₂ (dmit = 1,3-dithiole-2-thione-4,5-dithiolate)

Reizo Kato * and Cui Hengbo

Condensed Molecular Materials Laboratory, RIKEN, 2-1, Hirosawa, Wako-shi, Saitama, 351-0198, Japan; E-Mail: hcui@riken.jp (C.H.)

* Author to whom correspondence should be addressed; E-Mail: reizo@riken.jp; Tel.: +81-48-467-9408; Fax: +81-48-462-4661.

Received: 27 March 2012; in revised form: 25 June 2012 / Accepted: 27 June 2012 /

Published: 4 July 2012

Abstract: An isostructural series of anion radical salts, β' -(Et_xMe_{4-x}Z)[Pd(dmit)₂]₂ ($x = 0-2$, Z = P, As, Sb), with a quasi-triangular lattice comprising the dimer unit [Pd(dmit)₂]₂⁻ belong to a strongly correlated electron system with geometrical frustration. Intra and interdimer transfer integrals between the frontier molecular orbitals, which characterize the strength of electron correlation and degree of frustration, can be tuned by selection of the counter cation. We have systematically analyzed the crystal structure with X-ray diffraction method and intermolecular transfer integrals using extended Hückel molecular orbital calculations based on structural data. The variation in the cation affects the unit cell in a manner equivalent to an anisotropic pressure. Increasing the covalent radius of the central atom Z and the number of ethyl groups (x) in the cation leads to slight arching of the Pd(dmit)₂ molecule. This arch-shaped distortion of the Pd(dmit)₂ molecule modifies the interdimer transfer integrals in formation of the regular triangular dimer lattice. On the other hand, the intradimer transfer integral, which is correlated with the effective on-site Coulomb interaction of the dimer, is weakly dependent on the type of cation.

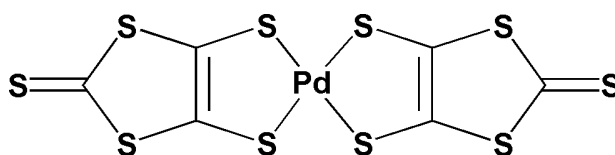
Keywords: molecular conductors; strongly correlated electron system; geometrical frustration; X-ray crystal structure analysis; transfer integrals

1. Introduction

Molecular conductors are notable for their simple and clear electronic structures. This means that simple tight-binding band calculations based on the extended Hückel method are quite useful for describing the energy bands in the vicinity of the Fermi level [1]. The conduction process in molecular conductors is governed by electron transfer between the frontier molecular orbitals; that is, the highest occupied molecular orbital (HOMO) or the lowest unoccupied molecular orbital (LUMO), and thus the transfer integrals between HOMOs or LUMOs determine the electronic structure. In the crystal state, the transfer integrals are generally sensitive to the molecular arrangement and orientation, because the component molecules belong to conjugated π systems with highly anisotropic molecular shapes. Another notable attribute of molecular conductors is the variety of chemical modifications that are possible, leading to a diversity of electronic properties and enabling their fine tuning. Most molecular conductors are classified as ion (cation or anion) radical salts composed of conducting and insulating parts. Notably, chemical modifications of the insulating part, as well as the conducting part, allow control of the electronic properties, because the insulating part can affect the molecular arrangement and orientation of the conducting part.

The metal dithiolene complex $\text{Pd}(\text{dmit})_2$ (dmit = 1,3-dithiole-2-thione-4,5-dithiolate; Figure 1) provides an isostructural series of anion radical salts, $\beta'-(\text{Et}_x\text{Me}_{4-x}\text{Z})[\text{Pd}(\text{dmit})_2]_2$ ($x = 0-2$, $Z = \text{P, As, Sb}$) [2–5]. Here, the monovalent counter cations, $\text{Et}_x\text{Me}_{4-x}\text{Z}^+$, form the insulating part while electrical conduction is attributed to the anion radical of $\text{Pd}(\text{dmit})_2$. In crystals of the β' -type $\text{Pd}(\text{dmit})_2$ salts, $\text{Pd}(\text{dmit})_2$ molecules form a dimer unit with one negative charge, $[\text{Pd}(\text{dmit})_2]_2^-$. The dimer units are networked to form a quasi-triangular lattice. At ambient pressure, they are Mott insulators, in which the electrons cannot move due to strong on-site Coulomb repulsion. Application of (hydrostatic or uniaxial) pressure enlarges the band width and leads to metallic and (frequently) superconducting states. In the Mott insulating state, the localized spins exhibit various ground states (antiferromagnetic long-range order [6], quantum spin liquid state [7–11], and non-magnetic charge-ordered state [12–14]), depending on the counter cation. In the background of all these transport and magnetic properties, electron correlation and geometrical frustration operate [3,6]. The strength of the electron correlation and degree of frustration are characterized by the intra- and interdimer transfer integrals between the frontier molecular orbitals [2,15]. These transfer integrals can be systematically tuned by selecting counter cations, $\text{Et}_x\text{Me}_{4-x}\text{Z}^+$, with different x (number of ethyl groups) and Z (central pnictogen atom). However, the observed effects of the counter cation on the structural properties of the $\text{Pd}(\text{dmit})_2$ site remain unclear. Herein, we report on the cation dependence of the crystal and molecular structures of β' -type $\text{Pd}(\text{dmit})_2$ salts and discuss their relation in terms of intermolecular transfer integrals.

Figure 1. Molecular structure of $\text{Pd}(\text{dmit})_2$.



2. Results and Discussion

2.1. Lattice Constants

Crystals of the β' -type $\text{Pd}(\text{dmit})_2$ salts belong to a monoclinic system with space group $C2/c$. The unit cell contains two crystallographically equivalent $\text{Pd}(\text{dmit})_2$ anion layers (1 and 2), which are separated by a cation layer (Figure 2). The $\text{Pd}(\text{dmit})_2$ layers are related by glide plane symmetry. The cations are located on a two-fold axis, and thus cations without two-fold symmetry (EtMe_3Z^+) may adopt two possible orientations with an occupancy of 50% for each orientation. In the $\text{Pd}(\text{dmit})_2$ layer, $\text{Pd}(\text{dmit})_2$ molecules are strongly dimerized with an eclipsed overlapping mode. The number of crystallographically independent dimer units is one. The two $\text{Pd}(\text{dmit})_2$ molecules in the dimer unit are equivalent and related by inversion symmetry. The dimer units stack along the $a + b$ direction in layer 1 and along the $a - b$ direction in layer 2 (Figure 2; solid-crossing column structure). Table 1 shows the lattice constants of β' - $(\text{Et}_x\text{Me}_{4-x}\text{Z})[\text{Pd}(\text{dmit})_2]_2$, plotted as a function of the covalent radius of the central atom Z (R_Z) in Figure 3. Understandably, the effect of the number of ethyl groups (x) is larger than that of R_Z in general. With decreasing R_Z and x , the unit cell volume V decreases. In this sense, the cation effect appears equivalent to an application of pressure. However, each lattice constant shows complicated behavior. In particular, in the ac plane, the lattice constants a and c exhibit opposite R_Z dependences, and the x dependence of the β angle gets weaker as R_Z increases. Overall, however, the area of the ac plane ($ac \sin\beta$) shows rather normal dependence on R_Z and x . All these results indicate that the cation effect on the unit cell is similar to the pressure effect but is not isotropic, which would be a feature of chemical pressure.

Figure 2. Crystal structure of the β' -type $\text{Pd}(\text{dmit})_2$ salt.

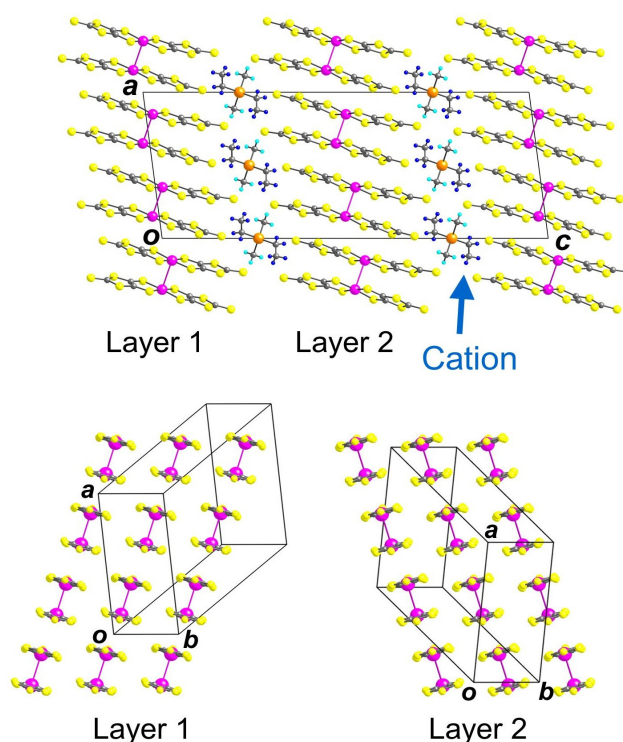


Figure 3. Lattice constants of β' -(Et_xMe_{4-x}Z)[Pd(dmit)₂]₂ plotted as a function of the covalent radius of the central atom Z (R_Z).

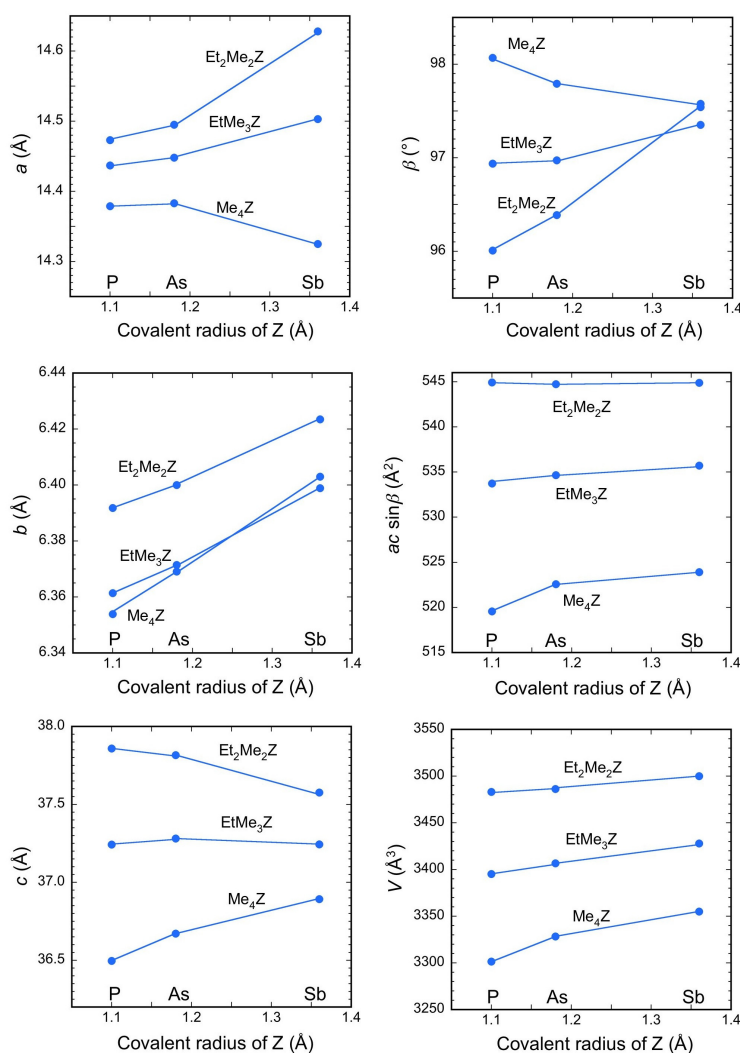


Table 1. Lattice constants of β' -(Cation)[Pd(dmit)₂]₂.

Cation	a (Å)	b (Å)	c (Å)	β (°)	V (Å ³)
Me ₄ P	14.379(3)	6.3539(12)	36.496(7)	98.070(2)	3301.5(11)
Me ₄ As	14.383(4)	6.3691(15)	36.672(9)	97.793(3)	3328.4(14)
EtMe ₃ P	14.437(4)	6.3614(15)	37.243(9)	96.938(3)	3395.3(14)
EtMe ₃ As	14.448(4)	6.3715(18)	37.282(11)	96.973(3)	3406.7(18)
Et ₂ Me ₂ P	14.473(3)	6.3918(13)	37.859(8)	96.009(3)	3483.1(13)
Et ₂ Me ₂ As	14.495(4)	6.4000(15)	37.816(10)	96.388(3)	3486.3(15)
Me ₄ Sb	14.325(7)	6.403(3)	36.893(19)	97.543(5)	3355(3)
EtMe ₃ Sb	14.503(3)	6.3989(12)	37.244(7)	97.352(2)	3427.9(12)
Et ₂ Me ₂ Sb	14.628(4)	6.4235(15)	37.577(9)	97.577(2)	3500.0(15)

2.2. Interdimer Transfer Integrals

In molecular conductors, including the present system, the electronic structure in the vicinity of the Fermi level is well described by the tight-binding method based on the extended Hückel molecular

orbital calculation. Intermolecular transfer integrals between frontier orbitals (in general, HOMOs in a donor system and LUMOs in an acceptor system) calculated from crystal data determine the energy bands around the Fermi level. Figure 4a shows a set of intermolecular transfer integrals for the β' -type $\text{Pd}(\text{dmit})_2$ salts. (Note here that the C -centered unit cell is reduced to a primitive cell that contains only one dimer in the anion layer. Interlayer interactions are weak, and thus neglected in this work). Although the $\text{Pd}(\text{dmit})_2$ molecule is an acceptor, the conduction band of the β' -type $\text{Pd}(\text{dmit})_2$ salts originates from the HOMO. This is a quite unique feature of this system, and is due to the small HOMO-LUMO energy gap, Δ , and the strong dimerization [16]. In the dimer unit, each HOMO and LUMO in the monomer forms bonding and antibonding pairs with a dimerization gap. The dimerization gap is expressed as $2|T_A|$, and both pairs have nearly the same gap value. In the β' -type $\text{Pd}(\text{dmit})_2$ salts, because $2|T_A|$ is larger than Δ , the antibonding HOMO pair is located above the bonding LUMO pair and forms a half-filled conduction band. The LUMO-based energy bands are located near the HOMO-based conduction band and play an important role, which is another unique feature of the present system. Hereinafter, however, we focus on the intermolecular HOMO-HOMO interactions that govern the electronic structure near the Fermi level. In Table 2, the intermolecular HOMO-HOMO transfer integrals are listed for all the salts.

Figure 4. End-on projections of the dimer lattice in β' -type $\text{Pd}(\text{dmit})_2$ salts showing labelling of (a) intermolecular transfer integrals and (b) interdimer transfer integrals.

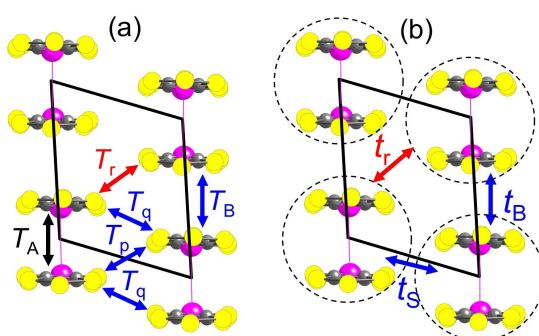


Table 2. Intermolecular highest occupied molecular orbital (HOMO)-HOMO transfer integrals in β' -(Cation)[$\text{Pd}(\text{dmit})_2$]₂ (See Figure 4a).

Cation	T_A (meV)	T_B (meV)	T_p (meV)	T_q (meV)	T_r (meV)
Me_4P	437	68.2	29.5	18.2	41.6
Me_4As	440	65.2	27.2	18.0	44.7
EtMe_3P	443	64.7	25.3	18.6	45.1
EtMe_3As	441	64.6	24.1	18.3	46.3
$\text{Et}_2\text{Me}_2\text{P}$	440	56.0	22.0	17.3	47.2
$\text{Et}_2\text{Me}_2\text{As}$	436	53.7	21.1	17.1	47.5
Me_4Sb	449	57.7	22.7	16.3	48.5
EtMe_3Sb	449	56.4	20.4	16.8	50.1
$\text{Et}_2\text{Me}_2\text{Sb}$	445	52.5	18.3	15.9	51.6

The strong dimerization allows us to take each dimer as an effective unit [2] and we can then redraw the unit cell with interdimer transfer integrals as shown in Figure 4b. In the dimer model, the

conduction band is described by three interdimer transfer integrals, t_B , t_S , and t_r , as listed in Table 3. The interdimer transfer integrals relate to the intermolecular transfer integrals in Table 2 as $t_B = T_B/2$, $t_S = (T_p + 2T_q)/2$, and $t_r = T_r/2$. The largest transfer integral, t_B or t_S , is correlated with the band width W . For each salt, the triangular lattice formed by the interdimer interactions is approximately isosceles ($t_B \approx t_S$), and thus the anisotropy of the triangular lattice can be estimated by the ratio t_r/t , where $t = (t_B + t_S)/2$. The anisotropy of the triangular lattice indicates the degree of geometrical frustration. As shown in Table 3 and Figure 5, t_r/t increases with increasing R_Z and x , and the $\text{Et}_2\text{Me}_2\text{Sb}$ salt has an almost regular triangular lattice. The R_Z and x dependences of t and t_r are plotted in Figure 6. The increasing tendency of t_r/t is a consequence of decreasing t and increasing t_r . The decrease in t may be reasonable given that any increase in R_Z or x would expand the lattice and lengthen the intermolecular distances. On the other hand, the increase in t_r indicates some non-trivial structural change. In this system, the intermolecular transfer integrals are governed mainly by the overlap between the p orbitals of the sulfur atoms in the dmit ligand. Figure 7 shows the relation between T_r and the intermolecular S...S distances responsible for T_r . Notably, an increase in T_r results in shortening of $d1$ and $d2$, associated with the outer heteroring, while $d3$ and $d4$, associated with the inner heteroring, remain almost constant or slightly lengthen. These trends cannot be explained by changes in the lattice constants. When the dimer is viewed along the vector connecting the two Pd atoms, we notice that the $\text{Pd}(\text{dmit})_2$ molecules in the dimer are not completely eclipsed (Figure 8). In particular, there is significant displacement of the outer parts, which indicates that the $\text{Pd}(\text{dmit})_2$ molecule is slightly arched, with both ends of the molecule slightly deviating from the expected linear axis. Indeed, the arch-shaped distortion of the molecule can be detected in the bond lengths and angles, for example, in the $\text{Et}_2\text{Me}_2\text{Sb}$ salt (Figure 9). In addition, Figure 8 suggests that the curvature depends on the counter cation. We tentatively describe the degree of arch-shaped distortion by defining the torsion angle of S–Pd–Pd–S (Φ) within the dimer (Figure 10). Figure 10 indicates that Φ changes systematically depending on the counter cation (R_Z and x), which is consistent with the above-mentioned trends for the intermolecular S...S distances.

Table 3. Interdimer HOMO-HOMO transfer integrals and band width, W , calculated in the dimer model (See Figure 4b).

Cation	t_B (meV)	t_S (meV)	t (meV)	t_r (meV)	t_r/t	W (meV)
Me_4P	34.1	32.9	33.5	20.8	0.620	271
Me_4As	32.6	31.6	32.1	22.3	0.696	264
EtMe_3P	32.3	31.3	31.8	22.5	0.709	262
EtMe_3As	30.5	30.3	30.4	23.2	0.761	254
$\text{Et}_2\text{Me}_2\text{P}$	28.0	28.3	28.1	23.6	0.839	240
$\text{Et}_2\text{Me}_2\text{As}$	26.9	27.6	27.2	23.8	0.873	235
Me_4Sb	28.8	27.7	28.3	24.2	0.858	243
EtMe_3Sb	28.2	27.0	27.6	25.0	0.907	241
$\text{Et}_2\text{Me}_2\text{Sb}$	26.3	25.1	25.7	25.8	1.005	231

Figure 5. Relation between anisotropy of the dimer lattice t_r/t (See Table 3), and the covalent radius of the central atom Z (R_Z).

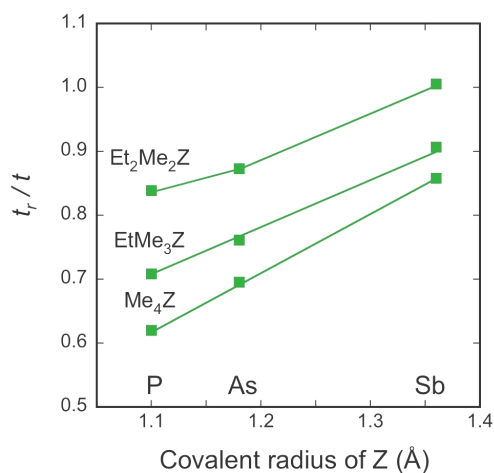


Figure 6. Intermolecular highest occupied molecular orbital (HOMO)-HOMO transfer integrals t and t_r (See Table 3) plotted as a function of the covalent radius of the central atom Z (R_Z).

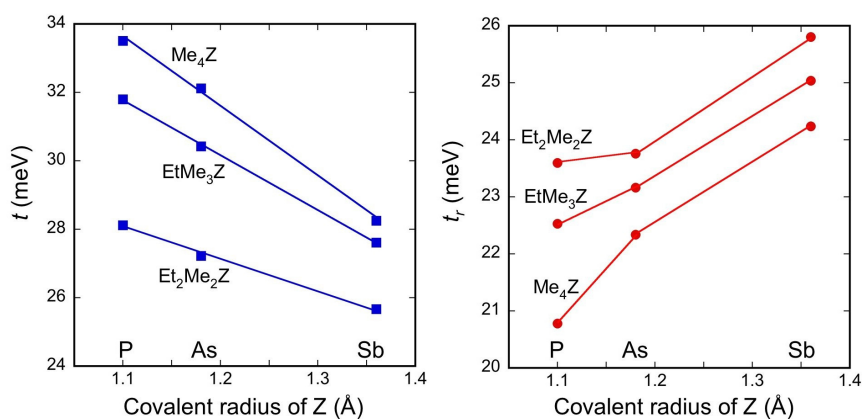


Figure 7. Relations between t_r and intermolecular S...S distances (Å) responsible for T_r .

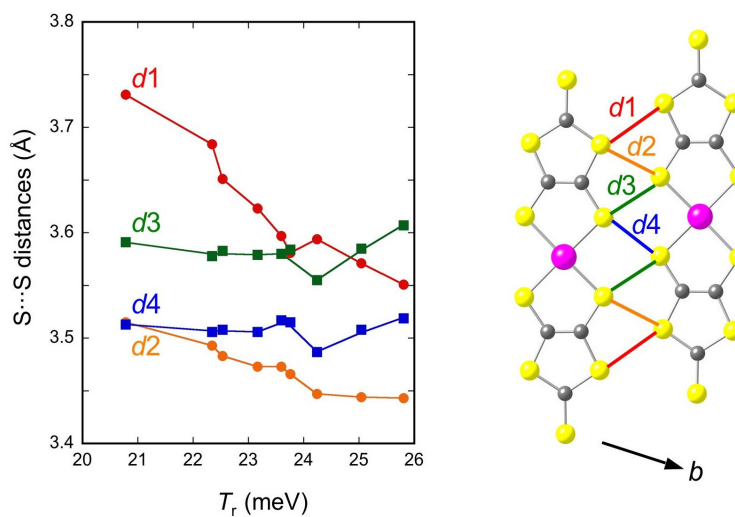


Figure 8. $[\text{Pd}(\text{dmit})_2]_2^-$ dimers viewed along the vector connecting the two Pd atoms in Me_4P , Me_4As , $\text{Et}_2\text{Me}_2\text{As}$, and $\text{Et}_2\text{Me}_2\text{Sb}$ salts.

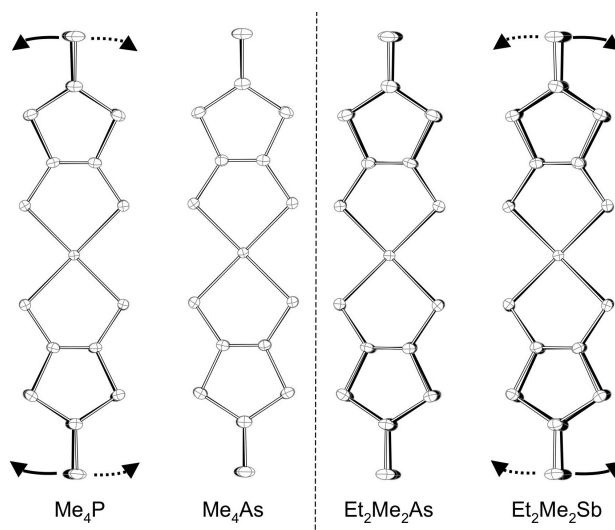


Figure 9. Bond lengths and angles of the $\text{Pd}(\text{dmit})_2$ unit in the $\text{Et}_2\text{Me}_2\text{Sb}$ salt.

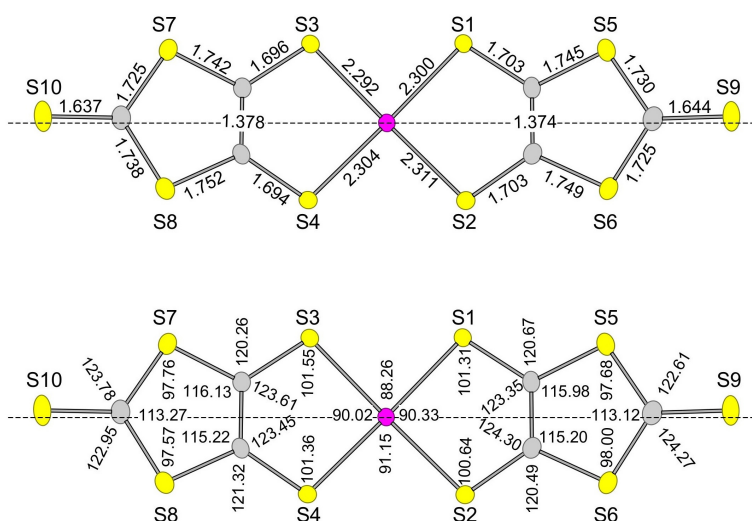
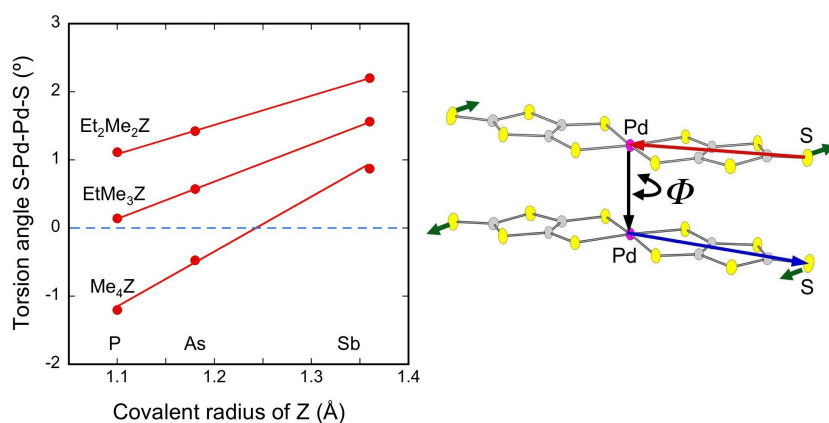


Figure 10. Relation between torsion angle of S-Pd-Pd-S (Φ) within the dimer and the covalent radius of the central atom Z (R_Z).



The arch-shaped distortion affects not only T_r but also the other intermolecular transfer integrals. With increasing cation size (R_Z and x), the $\text{Pd}(\text{dmit})_2$ molecule becomes distorted, as indicated by the green arrows in Figure 11. The distortion reduces the face-to-face overlap along the stacking direction that correlates with T_B (Figure 11). The distortion lengthens the intermolecular $\text{S}\cdots\text{S}$ contacts responsible for T_p , which is consistent with the observed relation between T_p and the intermolecular $\text{S}\cdots\text{S}$ distances responsible for T_p (Figure 12). In contrast to the results for T_r (Figure 7), a reduction in T_p correlates with elongation of all the $\text{S}\cdots\text{S}$ distances (Figure 12). As a result, the three interdimer transfer integrals, t_B , t_S , and t_r , are reasonably correlated with Φ (Figure 13).

Figure 11. End-on projection of the dimer lattice, in which the green arrows indicate the molecular distortions occurring with increasing cation size (R_Z and x). Overlapping modes associated with T_B for Me_4P and $\text{Et}_2\text{Me}_2\text{Sb}$ salts are also presented on the right side.

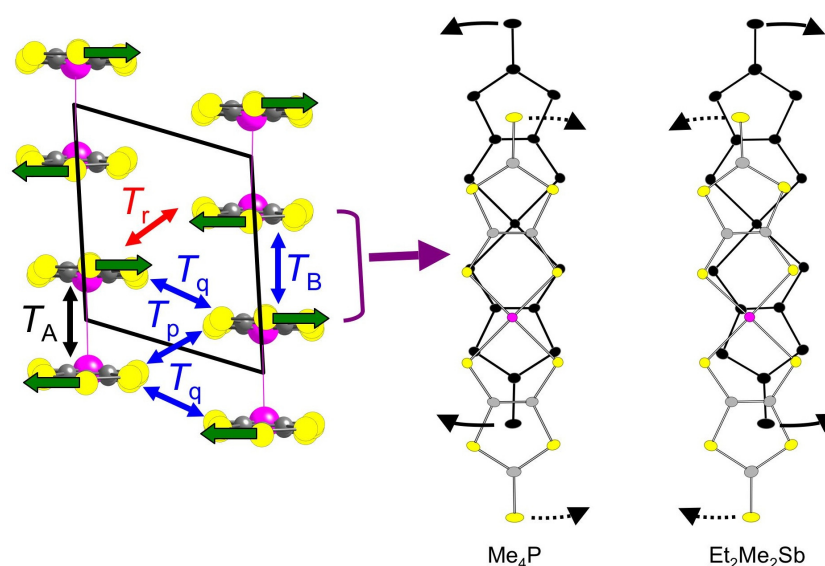


Figure 12. Relations between T_p and intermolecular $\text{S}\cdots\text{S}$ distances (\AA) responsible for T_p .

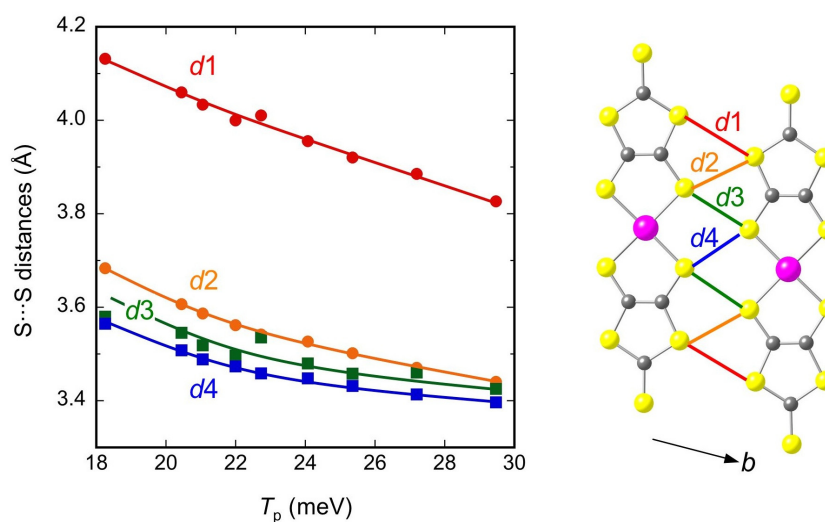
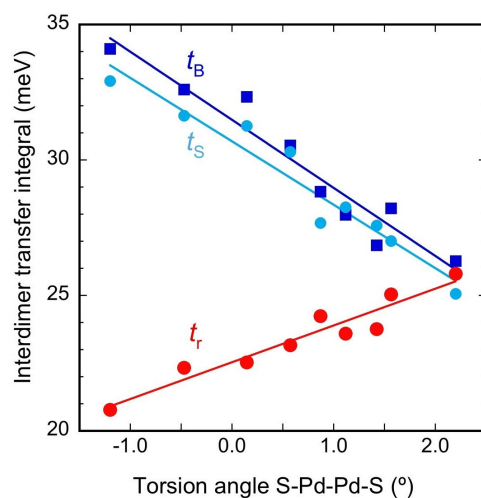


Figure 13. Interdimer transfer integrals as a function of the torsion angle of S–Pd–Pd–S (Φ).

2.3. Intradimer Transfer Integrals

In the Mott system based on dimer units, the intradimer transfer integral (T_A) is approximately correlated with the effective on-site Coulomb energy of the dimer [15]. Figure 14 shows the T_A values of β' -type Pd(dmit)₂ salts as a function of R_Z . Although the T_A values are larger than the interdimer transfer integrals, their variation is within 5%, which is smaller than the observed variations in t and t_r . As a result, we can say that the effect of the counter cation on T_A is relatively weak. The cation dependence of T_A appears complicated and does not show a systematic trend. In Figure 15, the intermolecular S...S distances responsible for T_A are plotted against T_A . (Note here that the T_A contribution of the Pd...Pd contact is small because the contribution of the d orbital of Pd to the HOMO is small). The inner S...S distances ($d1$ and $d2$) are shorter than the outer S...S distances ($d3$ and $d4$), which implies that the molecular plane is warped, as if the two Pd(dmit)₂ molecules in the dimer act to repel each other. For these two distinct groupings, the S...S distances are almost constant within each group over all the salts. The terminal S...S distances ($d5$) are largest and are slightly scattered without any clear tendency. The relation between T_A and Φ is shown in Figure 16, which suggests there are two distinct groups among the salts. The salts with $Z = \text{Sb}$ show larger T_A values, while the other salts ($Z = \text{P}, \text{As}$) exhibit a chevron-shaped Φ dependence. Since it is expected that the dimer with $\Phi = 0$ would have well-eclipsed overlapping modes, this chevron-shaped dependence on Φ seems reasonable. On the other hand, the origin of the larger T_A values for the Sb series remains an open question.

3. Experimental Section

Single crystals of β' -(Et_xMe_{4-x}Z)[Pd(dmit)₂]₂ were obtained by air oxidation of (Et_xMe_{4-x}Z)₂[Pd(dmit)₂] in acetone containing acetic acid. A typical procedure was as follows: (Et_xMe_{4-x}Z)₂[Pd(dmit)₂] (*ca.* 35 μmol) was dissolved in acetone (35–70 mL). After addition of acetic acid (4.0–5.5 mL), the resultant solution was allowed to stand at 5–10 °C for 3–4 weeks. The β' -type crystals (black elongated or hexagonal plates) were obtained as a single phase, with the exception of the EtMe₃P salt. The EtMe₃P salt contains a monoclinic $P2_1/m$ phase [17–21] as the main phase, and

triclinic- [22] and β' -phases (monoclinic $C2/c$) as minor phases. The β' -phase of the EtMe_3P salt was a very minor component.

Figure 14. Mapping of intradimer HOMO-HOMO transfer integrals T_A to the covalent radius of the central atom Z (R_Z).

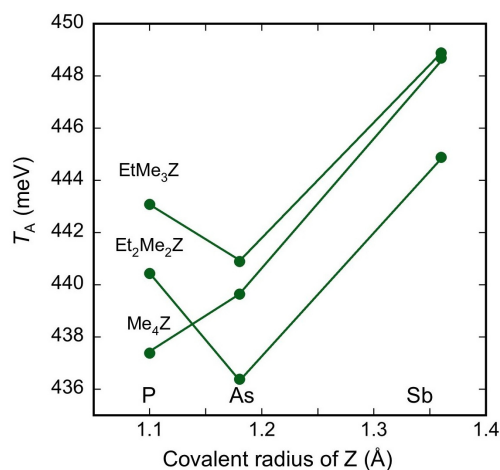


Figure 15. Relations between T_A and intermolecular S...S distances (Å) responsible for T_A .

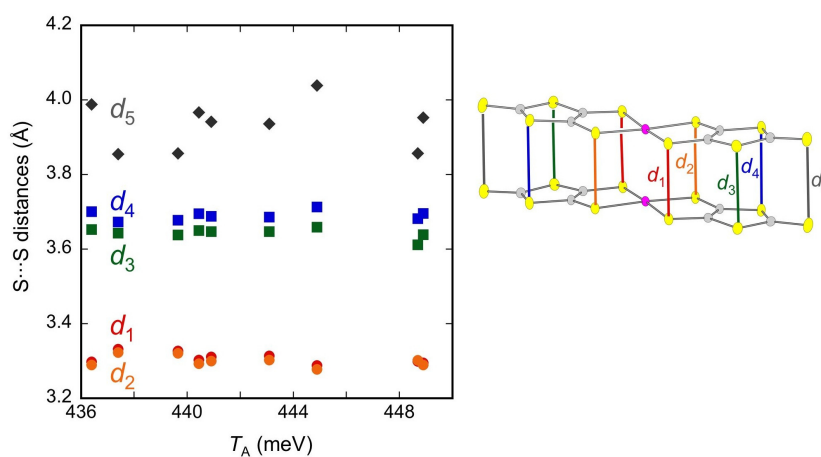
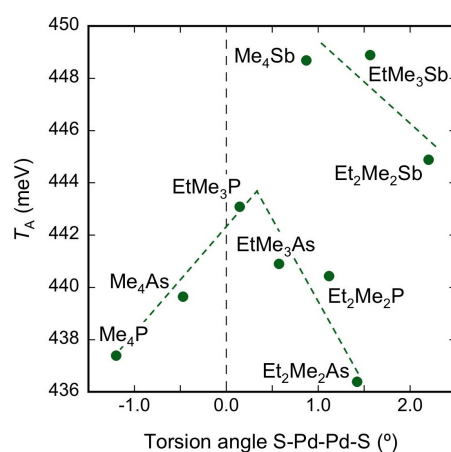


Figure 16. Mapping of intradimer HOMO-HOMO transfer integrals T_A to torsion angle of S-Pd-Pd-S (Φ).



X-ray diffraction data were collected using a Rigaku Mercury CCD AFC10 system with monochromated Mo $K\alpha$ radiation at room temperature. All structures were solved by a direct method (SIR92) [23] and refined on F^2 by the full-matrix least-squares method (SHELXL-97) [24]. Anisotropic atomic displacements were applied to all non-H atoms. The H atoms were placed at the calculated positions and refined by applying the riding model.

Intermolecular overlap integrals (S) between HOMOs were obtained using extended Hückel molecular orbital calculations based on structural data. Semi-empirical parameters for Slater-type atomic orbitals are summarized in Table 4. Intermolecular transfer integrals, t (eV), were estimated using the equation $t = -10S$ [1].

Table 4. Semi-empirical parameters for Slater-type atomic orbitals.

atom	orbital	I_p (Ryd)	ζ_1	ζ_2
C	2s	1.573	1.625	
	2p	0.838	1.625	
S	3s	1.620	2.122	
	3p	0.770	1.827	
Pd	5s	0.676	2.19	
	5p	0.390	2.15	
	4d	0.949	5.98	2.613
			(0.5264) *	(0.6372) *

* Contraction coefficients used in the double- ζ expansion.

4. Conclusions

The crystal structures of β^1 -type Pd(dmit)₂ salts corresponding to a two-dimensional Mott system with a quasi triangular lattice were investigated systematically, and the effects of the counter cation on intermolecular transfer integrals revealed. The intradimer transfer integral, which is correlated with the effective on-site Coulomb interaction of the dimer and the dimerization gap, weakly depends on the type of cation. On the other hand, the anisotropy of the triangular lattice (the ratio of interdimer transfer integrals, t_r/t), which determines the degree of frustration, can be tuned from 0.6 (Me₄P salt) to 1.0 (Et₂Me₂Sb salt) by changing the bulkiness of the cation (R_Z and x). An essential feature of the effect of the cation on the interdimer transfer integrals is the arch-shaped distortion observed in the Pd(dmit)₂ molecule rather than molecular rearrangement. That is, the Pd(dmit)₂ molecule is sufficiently flexible within the crystal field, allowing distortions of the molecular skeleton to occur with different counter cations, in turn leading to systematic changes in the intermolecular interactions. Understanding the origin of the arch-shaped molecular distortion is of considerable interest in materials design in such systems. In the present system, the counter cations are located discretely and there is no observable cation framework based on cation...cation interactions which can accommodate anions. Although some kind of cation...anion interaction would be expected, we did not identify any significant short contacts between cations and anions. Notably, structural optimization for atomic geometries calculated within the generalized gradient approximation can reproduce the arch-shaped molecular distortion and its cation dependence [25], which should provide important clues to its origin. Further studies are needed to clarify how the degree of molecular distortion is controlled by the counter cation in the crystal.

Acknowledgments

This research was partially supported by grant-in-aid for Scientific Research on Innovative Areas (No. 20110003) from the Ministry of Education, Culture, Sports, Science and Technology (MEXT), and by grant-in-aid for Scientific Research (S) (No. 22224006) from the Japan Society for the Promotion of Science (JSPS).

Conflict of Interest

The authors declare no conflict of interest.

References and Notes

1. Mori, T.; Kobayashi, A.; Sasaki, Y.; Kobayashi, H.; Saito, G.; Inokuchi, H. The intermolecular interaction of tetrathiafulvalene and bis(ethylenedithio)tetrathiafulvalene in organic metals. Calculation of orbital overlaps and models of energy-band structures. *Bull. Chem. Soc. Jpn.* **1984**, *57*, 627–633.
2. Kato, R. Conducting metal dithiolene complexes: Structural and electronic properties. *Chem. Rev.* **2004**, *104*, 5319–5346.
3. Tamura, M.; Kato, R. Variety of valence bond states formed of frustrated spins on triangular lattices based on a two-level System Pd(dmit)₂. *Sci. Technol. Adv. Mater.* **2009**, *10*, 024304:1–024304:12.
4. Tamura, M.; Kato, R. Spin-1/2 Heisenberg antiferromagnets on anisotropic triangular lattice, [Pd(dmit)₂] salts—How do they release frustration? *Polyhedron* **2005**, *24*, 2817–2820.
5. Kanoda, K.; Kato, R. Mott physics in organic conductors with triangular lattices. *Annu. Rev. Condens. Matter Phys.* **2011**, *2*, 167–188.
6. Tamura, M.; Kato, R. Magnetic susceptibility of β'-[Pd(dmit)₂] salts (dmit = 1,3-dithiol-2-thione-4,5-dithiolate, C₃S₅): Evidence for frustration in spin-1/2 Heisenberg antiferromagnets on a triangular lattice. *J. Phys. Condens. Matter.* **2002**, *14*, L729–L734.
7. Itou, T.; Oyamada, A.; Maegawa, S.; Tamura, M.; Kato, R. Quantum spin liquid in the spin-1/2 triangular antiferromagnet EtMe₃Sb[Pd(dmit)₂]₂. *Phys. Rev. B* **2008**, *77*, 104413:1–104413:5.
8. Itou, T.; Oyamada, A.; Maegawa, S.; Kato, R. Instability of a quantum spin liquid in an organic triangular-lattice antiferromagnet. *Nat. Physics* **2010**, *6*, 673–676.
9. Yamashita, M.; Nakata, N.; Senshu, Y.; Nagata, M.; Yamamoto, H.M.; Kato, R.; Shibauchi, T.; Matsuda, Y. Highly mobile gapless excitations in a two-dimensional candidate quantum spin liquid. *Science* **2010**, *328*, 1246–1248.
10. Kato, R.; Itou, T. Molecular quasi-triangular lattice antiferromagnets. In *Understanding Quantum Phase Transitions*; Lincoln, D.C., Ed.; CRC Press: Boca Raton, FL, USA, 2010; pp. 419–443.
11. Yamashita, S.; Yamamoto, T.; Nakazawa, Y.; Tamura, M.; Kato, R. Gapless spin liquid of an organic triangular compound evidenced by thermodynamic measurements. *Nature Commun.* **2011**, *2*, 275:1–275:6.
12. Tamura, M.; Kato, R. Valence instability in a dimer of two-orbital system: Possible charge separation due to “Negative *U*” effect. *Chem. Phys. Lett.* **2004**, *387*, 448–452.

13. Nakao, A.; Kato, R. Structural study of low temperature charge-separated phases of Pd(dmit)₂-based molecular conductors. *J. Phys. Soc. Jpn.* **2005**, *74*, 2754–2763.
14. Tamura, M.; Takenaka, K.; Takagi, H.; Sugai, S.; Tajima, A.; Kato, R. Spectroscopic evidence for the low-temperature charge-separated state of [Pd(dmit)₂] salts. *Chem. Phys. Lett.* **2005**, *411*, 133–137.
15. Tamura, M.; Kato, R. Effective on-site repulsion in molecular conductors with dimeric structure: Is the transfer integral a good measure of correlation? *J. Phys. Soc. Jpn.* **2004**, *73*, 3108–3110.
16. Canadell, E.; Ravy, S.; Pouget, J.P.; Brossard, L. Concerning the band structure of D[M(dmit)₂]₂ (D = TTF, Cs, NMe₄; M = Ni, Pd) molecular conductors and superconductors: Role of the M(dmit)₂ HOMO and LUMO. *Solid State Commun.* **1990**, *75*, 633–638.
17. Tamura, M.; Nakao, A.; Kato, R. Frustration-induced valence-bond ordering in a new quantum triangular antiferromagnet based on [Pd(dmit)₂]. *J. Phys. Soc. Jpn.* **2006**, *75*, 093701:1–093701:4.
18. Kato, R.; Tajima, A.; Nakao, A.; Tamura, M. Two pressure-induced superconducting anion radical salts exhibiting different spin states at ambient pressure. *J. Am. Chem. Soc.* **2006**, *128*, 10016–10017.
19. Ishii, Y.; Tamura, M.; Kato, R. Magnetic study of pressure-induced superconductivity in the [Pd(dmit)₂] salt with spin-gapped ground state. *J. Phys. Soc. Jpn.* **2007**, *76*, 033704:1–033704:4.
20. Shimizu, Y.; Akimoto, H.; Tsujii, H.; Tajima, A.; Kato, R. Mott transition in a valence-bond solid insulator with a triangular lattice. *Phys. Rev. Lett.* **2007**, *99*, 256403:1–256403:4.
21. Itou, T.; Oyamada, A.; Maegawa, S.; Kubo, K.; Yamamoto, H.M.; Kato, R. Superconductivity on the border of a spin-gapped Mott insulator: NMR studies of the quasi-two-dimensional organic system EtMe₃P[Pd(dmit)₂]₂. *Phys. Rev. B* **2009**, *79*, 174517:1–174517:6.
22. Yamamoto, T.; Nakazawa, Y.; Tamura, M.; Nakao, A.; Ikemoto, Y.; Moriwaki, T.; Fukaya, A.; Kato, R.; Yakushi, K. Intradimer charge disproportionation in triclinic-EtMe₃P[Pd(dmit)₂]₂ (dmit: 1,3-dithiole-2-thione-4,5-dithiolate). *J. Phys. Soc. Jpn.* **2011**, *80*, 123709:1–123709:4.
23. Altomare, A.; Cascarano, G.; Giacovazzo, C.; Gualardi, A.; Burla, M.C.; Polidori, G.; Camalli, M. SIR92—a program for automatic solution of crystal structures by direct methods. *J. Appl. Cryst.* **1994**, *27*, 435–435.
24. Sheldrick, G.M. A short history of SHELX. *Acta Crystallogr. Sect. A* **2008**, *64*, 112–122.
25. Tsumuraya, T.; Seo, H.; Miyazaki, T.; Kato, R. Frustrated Mott system on the quasi-triangular lattice, Pd(dmit)₂ salts; A first-principles study. *J. Phys. Soc. Jpn.* **2012**, to be submitted for publication.